CRYSTAL GROWTH & DESIGN

Article

pubs.acs.org/crystal

# Improving the Solubility of Lenalidomide via Cocrystals

Jia-Xi Song,[†] Yan Yan,[†] Jia Yao,[†] Jia-Mei Chen,*[,‡] and Tong-Bu Lu*[,†,‡]

[†]MOE Key Laboratory of Bioinorganic and Synthetic Chemistry, School of Chemistry and Chemical Engineering, Sun Yat-Sen University, Guangzhou 510275, China

[‡]School of Pharmaceutical Sciences, Sun Yat-Sen University, Guangzhou 510006, China

Supporting Information

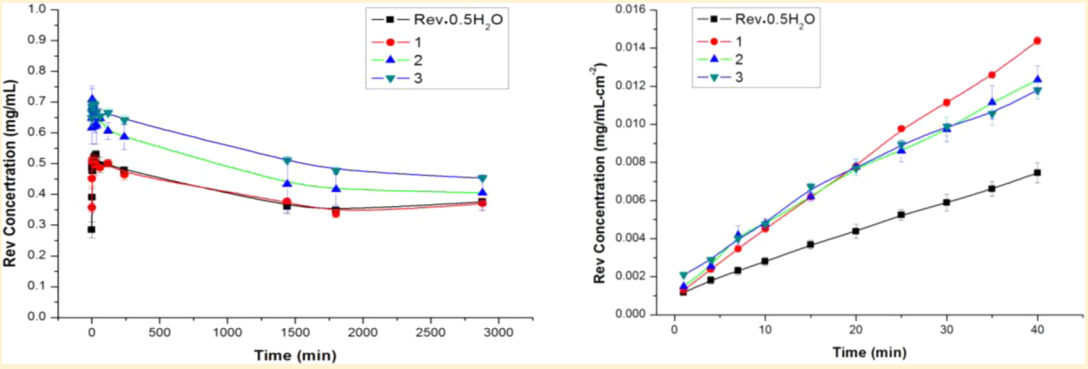


**ABSTRACT:** An anticancer drug, lenalidomide, has low oral bioavailability (below 33%) due to its poor solubility in water. To improve its solubility, three cocrystals of lenalidomide with urea (**1**) and 3,5-dihydroxybenzoic acid (**2**, **3**) were prepared. The structures of **1**−**3** were determined by single crystal X-ray diffraction, and they all form three-dimensional hydrogen-bonded frameworks between lenalidomide and the coformers. The apparent solubility value and intrinsic dissolution rate of lenalidomide in phosphate buffer of pH 6.8 have been improved after the formation of cocrystals. In addition, **2** and **3** can convert to each other under certain conditions.

## INTRODUCTION

Crystal engineering is the study of intermolecular interactions in the context of crystal packing and the utilization of such study to design new solids with desirable physicochemical properties.[1] In recent years, crystal engineering has played an important role in the area of the pharmaceutical industry and academia by means of exerting control on the intermolecular interactions to modify the physicochemical properties of active pharmaceutical ingredients (APIs).[2]

Pharmaceutical cocrystals are constructed from at least two molecules including an API and other solid components (referred to as coformers). The API and coformers in a cocrystal are neutral components rather than salts, in which the API and coformers are connected by noncovalent intermolecular interactions, such as hydrogen bonds, $\pi-\pi$ stacking, van der Waals forces, and halogen bonds.[3,4] Synthons are frequently used to evaluate the possibility of cocrystal formation in crystal engineering. Synthons are defined as structural units that represent the essential features of a crystal structure, which is also a simplification to analyze the stability and the variable interplay of thermodynamics and kinetics in the process of nucleation and early stages of crystallization. It is an enormous challenge in the prediction of crystal structures from molecular structures, and an important assumption is that the synthon is a reasonable approximation to the whole crystal.[5−8]

Lots of APIs have been eliminated from late-stage development as drug candidates because of their poor physicochemical properties, especially solubility, which pose a serious threat to clinical development.[9−11] Cocrystals have been identified as viable solid forms for improving the solubility of APIs and have become a research focus in the field of pharmaceutical materials.[12−16]

Lenalidomide, a thalidomide analogue, is an immunomodulatory agent with antiangiogenic and antineoplastic properties. It has been approved for the treatment of multiple myeloma and transfusion dependent anemia.[17] Lenalidomide is marketed under the trade name Revlimid (Rev). The commercially available form, Revlimid hemihydrate (Rev·0.5$H_2O$), has low oral bioavailability (below 33%) due to its poor solubility in water. Therefore, increasing the solubility of Rev and consequently improving its bioavailability by the formation of cocrystals is of interest for the development of new formulations of Rev.

As Rev contains one imide group, possible hydrogen bonding synthons containing imide group are shown in Scheme 1. Synthons I−IV[18,19] can be used for the construction of cocrystals of Rev. Therefore, a series of coformers containing

**Received:** March 5, 2014
**Revised:** April 24, 2014
**Published:** May 7, 2014

   dx.doi.org/10.1021/cg500327s | *Cryst. Growth Des.* 2014, 14, 3069−3077

**Scheme 1. Chemical Structures of Rev (left) and Possible Hydrogen Bonding Synthons of Rev with Coformers (right)**

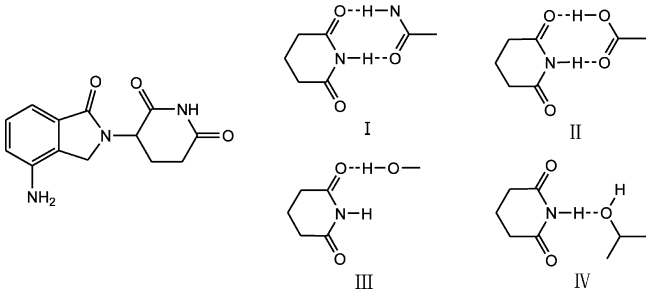


amide, carboxylic, and hydroxyl groups were used to interact with Rev (Table S1, Supporting Information), and three cocrystals of Rev with urea (**1**) and 3,5-dihydroxybenzoic acid (**2**, **3**) were successfully obtained. All the cocrystals were characterized by powder and single crystal X-ray diffraction, and their powder dissolution and intrinsic dissolution behavior were also investigated.

## EXPERIMENTAL SECTION

**Materials and General Methods.** Rev·0.5$H_2O$ was purchased from Zhejiang Taizhou Chemical Co. Ltd. Rev was acquired by heating Rev·0.5$H_2O$ to 150 °C and holding under this temperature for 1 h to remove the crystalline water. Urea and 3,5-dihydroxybenzoic acid (35DHBA) were purchased from Aladdin reagent Inc. All of the other chemicals and solvents were commercially available and used as received. The infrared spectra were recorded in the 4000 to 400 $cm^{-1}$ region using KBr pellets and a Bruker EQUINOX 55 spectrometer. X-ray powder diffraction (XRPD) patterns at room temperature were obtained on a Bruker D2 Advance with Cu K$\alpha$ radiation (30 kV, 10 mA), and variable temperature X-ray powder diffraction patterns (VT-XRPD) were obtained on a Bruker D8 Advance with Cu K$\alpha$ radiation (40 kV, 40 mA), with a heating rate of 10 °C/min and holding the measured temperature for 5 min for data collection. Thermogravimetric analyses (TGA) were recorded on a Netzsch TG-209 instrument and alumina crucible in nitrogen atmosphere, with a heating rate of 10 °C/min. Differential scanning calorimetry (DSC) was recorded on a Netzsch DSC 200 F3 instrument and aluminum sample pans in nitrogen atmosphere, with a heating rate of 5 °C/min.

**Grinding.** The cocrystals were prepared using liquid-assisted grinding (LAG)[20] method at room temperature. The experiment was performed by mixing stoichiometric amount of Rev (1 mmol) or Rev·0.5$H_2O$ (1 mmol) and coformers with appropriate solvent. The mixture was ground with a Retsch Mixer Mill model MM200 in a 25 mL stainless steel grinding jar and one stainless steel grinding ball (15 mm in diameter) at a frequency of 20 Hz for 30 min.

*Rev/Urea Cocrystal (1:1),* ***1****.* The cocrystal was prepared by grinding Rev·0.5$H_2O$ (268 mg, 1 mmol) and urea (60 mg, 1 mmol) with two drops of ethanol. The resulting solid was added to 3 mL of ethyl acetate and then allowed to slurry for 30 min. The suspension was filtered and the isolated solid of **1** was dried under a vacuum for 24 h at ambient temperature. The filtrate was left to evaporate slowly at room temperature in a sealed glass desiccator containing $P_2O_5$. After 3 days, block-shaped crystals of **1** were obtained. IR data (KBr, $cm^{-1}$): 3407, 3338, 3231, 3032, 2818, 1711, 1664, 1604, 1479, 1344, 1242, 927, 741, 676, 617.

*Rev/35DHBA Cocrystal (1:1),* ***2****.* The cocrystal was prepared by a procedure similar to that of **1**, except using 35DHBA instead of urea. Block-shaped crystals of **2** were obtained. IR data (KBr, $cm^{-1}$): 3388, 3245, 3072, 2656, 1706, 1600, 1490, 1426, 1336, 1290, 1205, 1164, 1007, 872, 754, 602.

*Rev/35DHBA Cocrystal Monohydrate (1:2:1),* ***3****.* The cocrystal was prepared by grinding Rev·0.5$H_2O$ (268 mg, 1 mmol) and 35DHBA (308 mg, 2 mmol) with one drop of water. The resulting solid was added to 4 mL of ethyl acetate and then allowed to slurry for 30 min. The suspension was filtered and the isolated solid of **3** was dried under a vacuum for 24 h at ambient temperature. The filtrate was evaporated slowly at room temperature in a sealed brown glass desiccator containing $P_2O_5$. After 5 days, noodle-shaped crystals of **3** were obtained. IR data (KBr, $cm^{-1}$): 3569, 3382, 3220, 2663, 1692, 1601, 1431, 1377, 1169, 1012, 905, 819, 737, 605.

**Single Crystal X-ray Diffraction.** Single-crystal X-ray diffraction data for cocrystals **1**−**3** were collected on an Agilent Technologies Gemini A Ultra system with graphite monochromated Cu K$\alpha$ radiation ($\lambda$= 1.54178 Å). Cell refinement and data reduction were applied using the program of CrysAlis PRO. The structures were solved by the direct methods using the SHELX-97 program[21] and

**Table 1. Crystallographic Data for 1−3**[a]

| | 1 | 2 | 3 |
|---|---|---|---|
| formula | $C_{14}H_{17}N_5O_4$ | $C_{20}H_{19}N_3O_7$ | $C_{27}H_{27}N_3O_{12}$ |
| formula weight | 319.33 | 413.38 | 585.52 |
| temperature/K | 285(14) | 150.00(10) | 150.01(10) |
| crystal system | monoclinic | triclinic | triclinic |
| space group | $P2_1/a$ | $P\bar{1}$ | $P\bar{1}$ |
| $a$, Å | 13.1592(6) | 8.6430(7) | 9.3808(7) |
| $b$, Å | 9.5499(3) | 8.9364(7) | 9.4520(7) |
| $c$, Å | 13.1773(6) | 13.4003(10) | 15.2326(9) |
| $\alpha$, deg | 90 | 86.348(6) | 96.684(5) |
| $\beta$, deg | 116.414(6) | 79.738(7) | 97.284(5) |
| $\gamma$, deg | 90 | 65.391(8) | 105.658(6) |
| $V$, Å$^3$ | 1483.09(11) | 925.88(13) | 1273.88(15) |
| $Z$ | 4 | 2 | 2 |
| $D_c$/g·cm$^{-3}$ | 1.430 | 1.483 | 1.526 |
| $F$(000) | 672 | 432 | 612 |
| range of indices | −15, 14; −8, 11; −15, 14 | −8, 9; −8, 10; −11, 15 | −10, 8; −10, 10; −14, 17 |
| $R_{int}$ | 0.0458 | 0.0314 | 0.0300 |
| GOF | 1.047 | 1.040 | 1.041 |
| $R_1$ [$I > 2\sigma(I)$] | 0.0445 | 0.0498 | 0.0493 |
| w$R_2$ [all data] | 0.1092 | 0.1245 | 0.1373 |

[a] $R_1 = \Sigma||F_o| - |F_c||/\Sigma|F_o|$. $wR_2 = [\Sigma[w(F_o^2 - F_c^2)^2]/\Sigma w(F_o^2)^2]^{1/2}$, $w = 1/[\sigma^2(F_o)^2 + (aP)^2 + bP]$, where $P = [(F_o^2) + 2F_c^2]/3$.


dx.doi.org/10.1021/cg500327s | Cryst. Growth Des. 2014, 14, 3069−3077

refined by the full-matrix least-squares method on $F^2$. All non-hydrogen atoms were refined with anisotropic displacement parameters. The hydrogen atoms were placed in calculated positions with fixed isotropic thermal parameters and included in the structure factor calculations in the final stage of full-matrix least-squares refinement. Crystallographic data and details of refinements of **1**−**3** are listed in Table 1, and the hydrogen bonding distances and angles are given in Table 2.

**Table 2. Hydrogen Bonding Distances and Angles for 1−3**

| D−H···A | D···A (Å) | D−H···A (deg) |
|---|---|---|
| **1**[a] | | |
| N3−H3···O5 | 2.832(2) | 177(2) |
| N1−H2···O1#1 | 2.949(3) | 167(2) |
| N1−H1···O2#2 | 3.167(3) | 148(3) |
| N5−H7···O1#3 | 2.877(2) | 172(2) |
| N5−H6···O5#4 | 2.937(3) | 178(3) |
| N4−H4···O2 | 3.032(3) | 167(2) |
| N4−H5···N1#5 | 3.361(3) | 148(3) |
| **2**[b] | | |
| N3−H3···O4#1 | 2.949(3) | 166(3) |
| N1−H1A···O5#2 | 3.324(3) | 150(3) |
| N1−H1B···O1#3 | 2.788(3) | 116(3) |
| N1−H1B···O2#4 | 3.251(3) | 152(3) |
| O6−H6···O7#5 | 2.601(2) | 176.7 |
| O4−H4···O3 | 2.749(3) | 172.9 |
| O5−H5···N1#6 | 2.809(3) | 166.7 |
| **3**[c] | | |
| O4−H13···O9 | 2.574(2) | 174.9 |
| O6−H16···O3#1 | 2.722(2) | 172.8 |
| O7−H18···N1#2 | 2.827(3) | 170.6 |
| O10−H24···O12#3 | 2.623(2) | 174.4 |
| O8−H19···O5 | 2.692(2) | 178.5 |
| O11−H21···O5#4 | 2.794(2) | 158.5 |
| O12−H25···O1#5 | 2.775(3) | 167(4) |
| O12−H26···O7 | 2.990(3) | 136(3) |
| O12−H26···O10#6 | 3.103(3) | 121(3) |
| N1−H1···O2#2 | 3.028(3) | 156(2) |
| N1−H2···O10#7 | 3.119(3) | 152(3) |
| N3−H3···O6 | 2.975(3) | 179(3) |

[a]Symmetry codes. #1 $x-1/2,-y+3/2,z$; #2 $-x+3/2,y+1/2,-z+2$; #3 $x-1/2,-y+1/2,z$; #4 $-x+1,-y,-z+1$; #5 $x,y-1,z$. [b]#1 $-x+1,-y+1,-z+1$; #2 $-x+1,-y+2,-z+1$; #3 $x+1,y,z$; #4 $-x+2,-y+1,-z+2$; #5 $-x,-y+3,-z+1$; #6 $x-1,y,z-1$. [c]#1 $-x,-y+2,-z+1$; #2 $-x-1,-y+1,-z$; #3 $x+1,y,z+1$; #4 $-x+1,-y,-z+1$; #5 $x,y-1,z$; #6 $-x+1,-y+1,-z+1$; #7 $-x,-y+1,-z+1$ (D and A are hydrogen bond donors and acceptors).

**High Performance Liquid Chromatography (HPLC) Analysis.** The contents of Rev were analyzed by a Shimadzu LC-20A HPLC system, with a C18 column (Inertsil ODS-3, 5 μm × 4.6 mm × 150 mm column, GL Sciences Inc., Japan) and a UV detection wavelength of 304 nm. The mobile phase consisted of acetonitrile/$H_2O$ (90/10, v/v) for **1** and acetonitrile/0.1% phosphoric acid (88/12, v/v) for **2** and **3**, with a flow rate of 1.0 mL/min.

**Powder Dissolution Experiments.** Concentrations of **1**−**3** and Rev·0.5$H_2O$ in 0.2 M phosphate buffer of pH 6.8 were determined by HPLC analysis, and peak area values were related to solution concentrations using a calibration curve. The solids were milled to powders and sieved using standard mesh sieves to provide samples with approximate particle size ranges of 75−150 μm. In a typical experiment, 50 mL of phosphate buffer was added to a flask containing 134 mg of Rev·0.5$H_2O$ (or corresponding to, for cocrystals **1**−**3**), and the resulting mixture was stirred at 37 °C and 500 rpm. At each time interval, an aliquot of the slurry was withdrawn from the flask and filtered through a 0.22 μm nylon filter. Appropriate dilutions were made to maintain absorbance readings within the standard curve. After the dissolution experiment, the remaining solid was collected by filtration, dried, and analyzed by XRPD, and the pH value of the resulting solution was also measured.

**Intrinsic Dissolution Measurement.** The intrinsic dissolution rate (IDR) experiments of solid materials were carried out on a ZQY-2 Dissolution Tester (Shanghai Huanghai Yaojian instrument distribution Co., Ltd.). Approximate 80 mg of each solid was compressed in a hydraulic press at 0.5 t for 2 s in a die of 5 mm diameter disk. The disk was coated using paraffin wax, leaving only the surface under investigation free for dissolution. Then the disk was dipped into 900 mL of 0.02 M phosphate buffer (pH 6.8) at 37 °C, with the paddle rotating at 100 rpm. At each time interval, 2 mL of the dissolution medium was withdrawn and replaced by an equal volume of fresh medium to maintain a constant volume. After filtration through a 0.22 μm nylon filter, solutions were injected into the HPLC system for analysis.

**Dynamic Vapor Sorption (DVS).** DVS study was performed on a DVS Intrinsic instrument (Surface Measurement Systems, UK). All samples were initially dried for several hours under a stream of nitrogen to establish the equilibrium dry mass under 25 °C. Then the relative humidity (RH) was increased in 10% RH steps to 95% RH. Finally, the RH was decreased in a similar fashion for the desorption phase. The temperature was maintained at a constant of 25 ± 0.1 °C. The sorption/desorption isotherms were calculated from the equilibrium mass values.

## RESULTS AND DISCUSSION

**Crystal Structures.** The asymmetric unit of **1** contains one urea and one Rev molecules, in which the urea molecules alternately link the Rev molecules through N3−H3···O5 and N4−H4···O2 (synthon I), and N5−H7···O1#3 intermolecular hydrogen bonds to form a wave-shaped chain along the *a* axis (Figure 1a). The adjacent chains are further connected via two interchain hydrogen bonds to generate a two-dimensional (2D) sheet along the *b* axis (Figure 1b), in which two hydrogen bonds are formed between the adjacent two Rev molecules (N1−H2···O1#1). The 2D sheets are further held together through three hydrogen bonds (N1−H1···O2#2, N5−H6···O5#4 and N4−H5···N1#5) and $\pi\cdots\pi$ interactions to form a three-dimensional (3D) structure of **1**, with the centroid···centroid distance of 3.671 Å (Figure 1c).

Similar to **1**, the asymmetric unit of **2** contains one 35DHBA and one Rev molecules, in which the 35DHBA molecules alternately link the Rev molecules through O4−H4···O3 (synthon III) and O5−H5···N1#6 intermolecular hydrogen bonds to form a chain along the *c* axis (Figure 2a). Two adjacent chains are connected with each other through N3−H3···O4#1 hydrogen bonds (synthon IV) and interchain hydrogen bonds (O6−H6···O7#5) to generate a 2D sheet along the *b* axis (Figure 2b). The 2D sheets are further held together through three hydrogen bonds (N1−H1A···O5#2, N1−H1B···O1#3 and N1−H1B···O2#4) to form a 3D structure (Figure 2c).

In contrast to **1** and **2**, the asymmetric unit of **3** contains one Rev, two 35DHBA and one water molecules, in which two 35DHBA molecules form a dimer through O4−H13···O9 and O8−H19···O5 intermolecular hydrogen bonds. Two dimers and one Rev molecule are linked by a water molecule through O12−H26···O7, O12−H26···O10#6 and O12−H25···O1#5 intermolecular hydrogen bonds to form a chain along the *c* axis. The adjacent chains are further connected via interchain hydrogen bonds (N3−H3···O6, synthon IV) to generate a 2D sheet along the *b* axis (Figure 3b). The 2D sheets are further held together through additional hydrogen bonds (O6−H16···


dx.doi.org/10.1021/cg500327s | Cryst. Growth Des. 2014, 14, 3069−3077

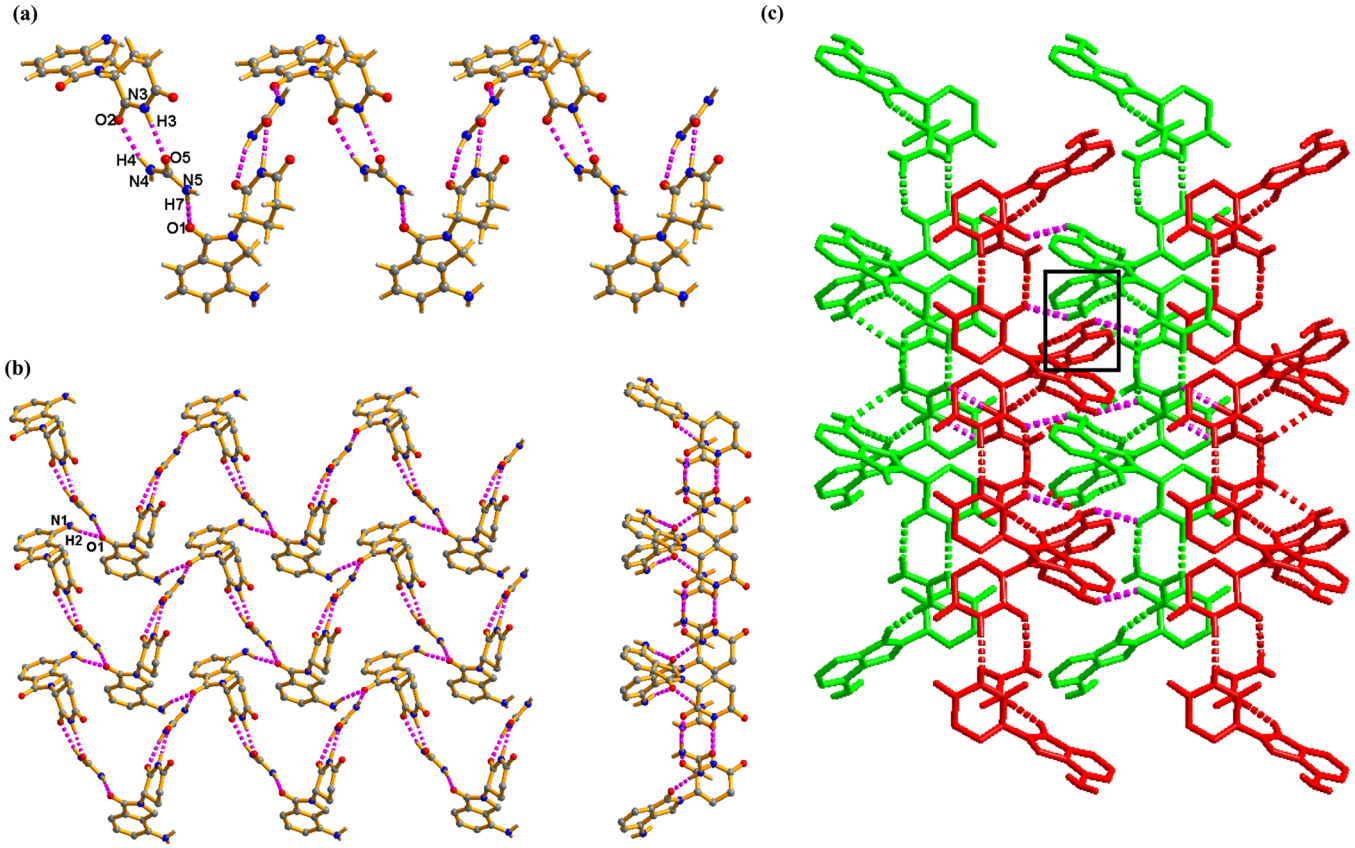


**Figure 1.** (a) 1D chain, (b) front view (left) and side view (right) of 2D sheet, and (c) 3D structure with $\pi\cdots\pi$ interactions (showing in the black box) of **1**.

O3#1, O7−H18···N1#2, O10−H24···O12#3, O11−H21···O5#4, N1−H1···O2#2 and N1−H2···O10#7) to form the 3D structure of **3** (Figure 3c).

**XRPD Analyses.** XRPD was used to check the crystalline phase purity of **1**−**3**. The results show that the patterns of the products are different from either that of API or those of corresponding coformers (Figure S1, Supporting Information), indicating the formation of new crystalline phases. In addition, all the peaks displayed in the measured patterns for **1**−**3** closely match those in the simulated patterns generated from single crystal diffraction data (Figure S1, Supporting Information), confirming the single phases of **1**−**3** were formed.

*Transformation between 2 and 3.* When slurring excess solids of **2** in acetonitrile/water containing saturated 35DHBA for 30 min, the XRPD analysis of the resulting solids indicates that **2** transforms to **3** in water while retaining its crystal form in acetonitrile (Figure S2, Supporting Information). The transformation process from **2** to **3** may involve the dissolution of **2** first, followed by the crystallization of **3** from the solution containing excess of 35DHBA in the presence of water, and the stoichiometry of 35DHBA/Rev increased from 1:1 in **2** to 2:1 in **3**. However, when the filtrate of the above acetonitrile solution of **2** and saturated 35DHBA was left to evaporate slowly at room temperature, crystals of **3** were obtained within 3−5 days at 25 °C, with the aid of water coming from the air and/or solvent (Figure S2, Supporting Information).

The TGA and DSC curves for **1**−**3** are shown in Figure 4. **1** and **2** begin to melt at 181 and 190 °C, respectively, accompanied by decomposition of Rev. The TGA curve of **3** shows a weight loss starting at 110 °C (Figure 4c); the weight loss of 3.1% from 110 to 140 °C for **3** is consistent with the loss of one $H_2O$ molecule (calcd 3.1%). The DSC curve of **3** shows two endothermic peaks between 100 and 160 °C. The first peak from 100 to 140 °C is attributed to the process of dehydration. The second small peak from 140 to 160 °C is related to a phase transition from **3** to **2**. There would be excess 35DHBA present as the 35DHBA/Rev ratio goes from 2:1 in **3** down to 1:1 in **2**. We collected DSC data of **3** up to 170 °C (Figure S4a, Supporting Information), and then immediately stopped heating and took the resulting sample to perform the XRPD measurement. The results of XRPD analysis (Figure S4b, Supporting Information) indicate that **3** indeed transforms to **2** and excess 35DHBA. The VT-XRPD patterns of **3** show that **3** maintains its crystallinity up to 100 °C, and then it begins to transform to **2** and 35DHBA at 105 °C, and the transformation process complete below 115 °C (Figure 5). After cooling to 30 °C, the mixture of **2** and 35DHBA could not convert back to **3** (Figure 5). The different transformation temperature display in DSC and VT-XRPD is due to the different heating rates during DSC and VT-XRPD measurements, 5 °C/min for DSC, and 10 °C/min (and holding each measured temperature for 5 min) for VT-XRPD.

The influence of humidity on the stability of **2** and **3** was studied by a DVS experiment. **3** uptakes 1.2% water at 95% RH, and a small hysteresis loop is observed (Figure 6), and then it loses the absorbed water near 0% RH. The crystalline water molecule in **3** is not lost even at 0% RH. The XRPD pattern for **3** after the DVS experiment also demonstrates that **3** is stable at 0% RH, and it does not lose its crystalline water and convert to **2** or other anhydrous forms (Figure S5a, Supporting


dx.doi.org/10.1021/cg500327s | *Cryst. Growth Des.* 2014, 14, 3069−3077

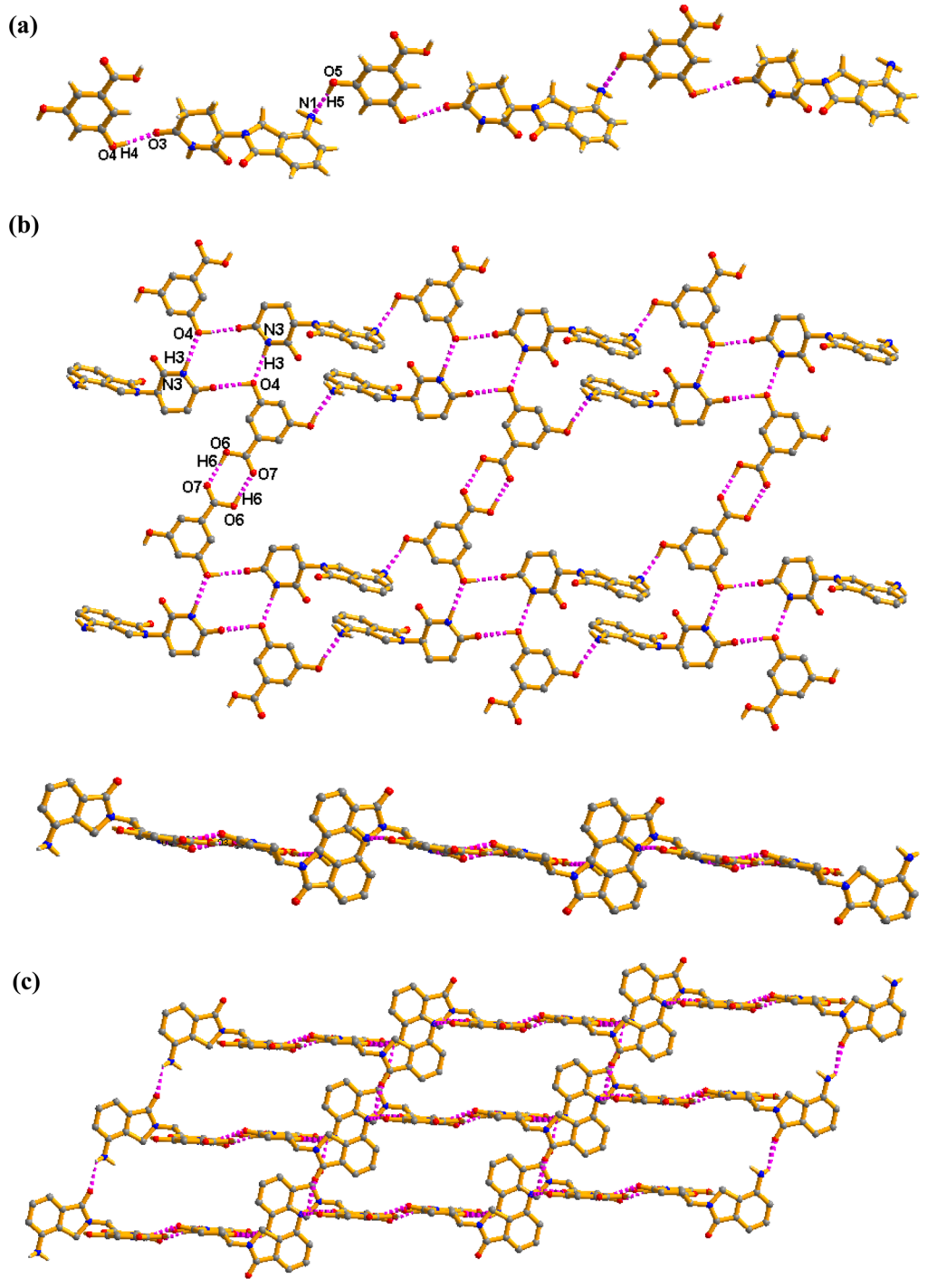


**Figure 2.** (a) 1D chain, (b) front view (up) and top view (down) of 2D sheet, and (c) 3D structure of **2**.

Information). Similar to **3**, **2** uptakes 1.7% water at 95% RH, and it is also stable and retains its crystal form after the DVS experiment (Figure S5b, Supporting Information).

**Powder Dissolution and IDR Studies.** Apparent solubility and dissolution rate of the solids are of paramount importance in pharmaceutical development as well as quality control, and shorter dissolution time and higher apparent solubility may result in more absorption.[22−25] Powder dissolution profiles for Rev·0.5$H_2O$ and **1**−**3** are shown in Figure 7a. It can be found that the maximum solubility values for **2** and **3** are approximately 1.4 times as large as that of Rev·0.5$H_2O$, while **1** displays dissolution behavior similar to Rev·0.5$H_2O$.

All these crystal forms reach their maximum solubility ($S_{max}$) within 3 min and then decrease slowly over time. This specific type of profile is a product of the "spring and parachute effect", which has been exhibited by many pharmaceutical cocrystals.[26−29] The supersaturated solution of Rev is formed at the initial stage of dissolution and then is preserved for several hours (Figure 7b). Such a behavior is especially favorable for pharmaceutical applications.[22] After 48 h (2880 min), the Rev concentrations of all the crystal forms are close to each other (Figure 7b), indicating all of them slowly transform to a more


dx.doi.org/10.1021/cg500327s | *Cryst. Growth Des.* 2014, 14, 3069−3077

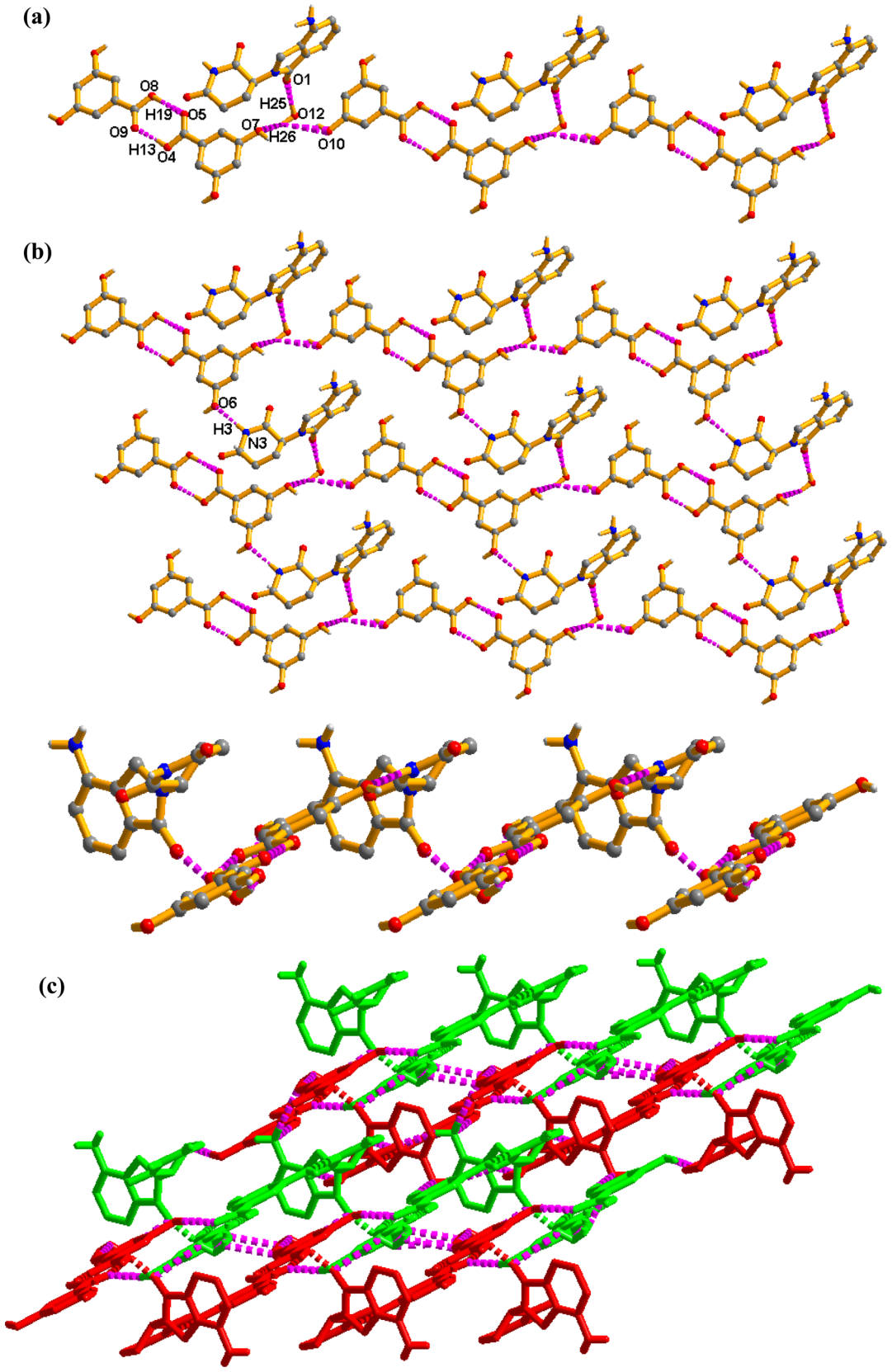


**Figure 3.** (a) 1D chain, (b) front view (up) and top view (down) of 2D sheet, and (c) 3D structure of **3**.

stable form of Rev. The slight difference in their concentrations at 48 h may be attributed to the small pH variation of the resulting solutions. Indeed, the pH values of the resulting solutions for Rev·0.5$H_2O$ and **1**−**3** after the powder dissolution experiments were measured, and a pH variation of ±0.13 was observed. The undissolved solids were filtered and dried under a vacuum, and the results of XRPD analyses indicate that all of them transformed to Rev·2$H_2O$[30] (Figures S6 and S7,


dx.doi.org/10.1021/cg500327s | *Cryst. Growth Des.* 2014, 14, 3069−3077

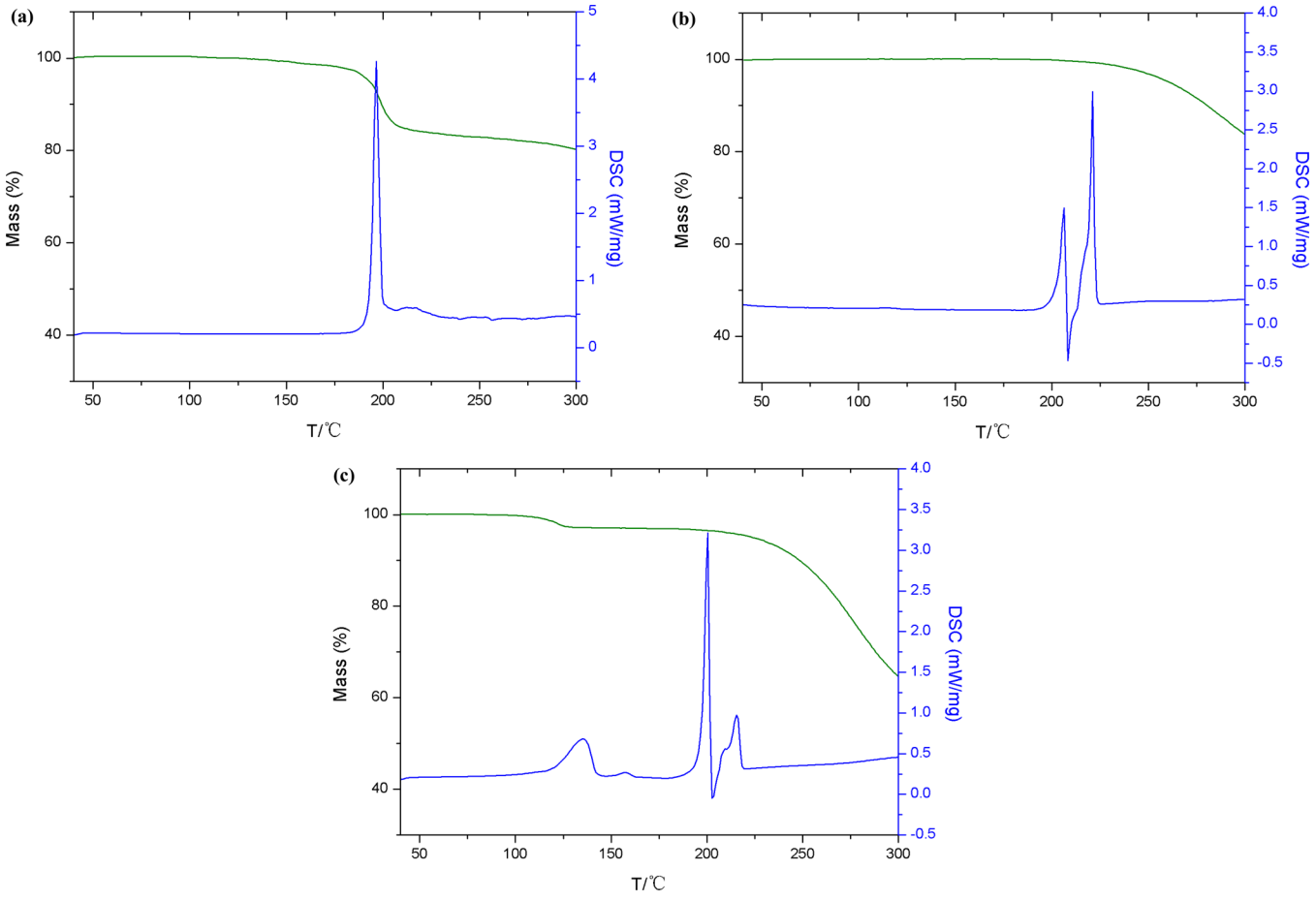


**Figure 4.** TGA and DSC curves for (a) **1**, (b) **2**, (c) **3**.

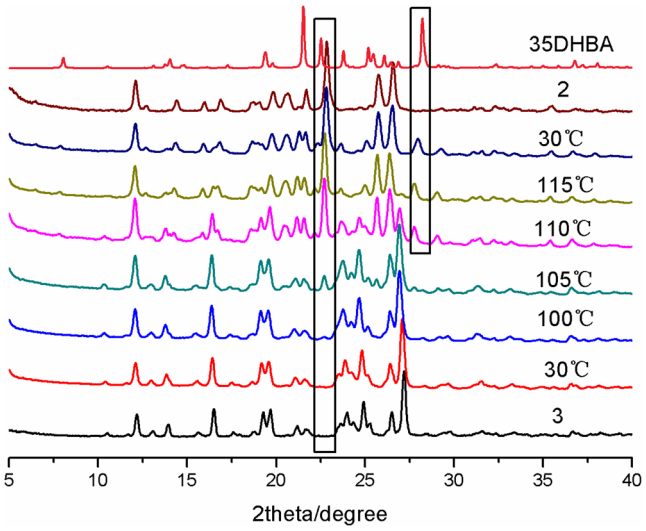


**Figure 5.** Variable temperature XRPD patterns for **3**.

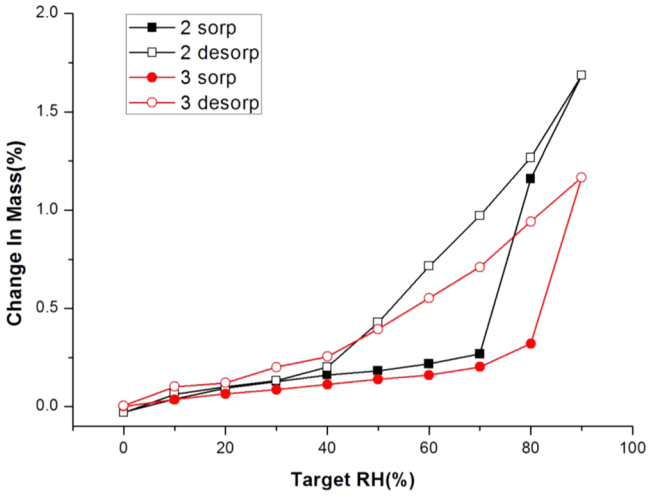


**Figure 6.** Water sorption/desorption isotherms for **2** and **3** at 25 °C.

Supporting Information). The solubility of Rev·$2H_2O$ is lower than that of Rev·$0.5H_2O$, and this is the reason why the concentration of Rev for Rev·$0.5H_2O$ also went down along with the dissolution time. XRPD analysis of the solids at earlier time points in powder dissolution experiments show the transformation of all crystal forms to Rev·$0.5H_2O$ in the first 3 min, followed by the further transformation to Rev·$2H_2O$ with different speeds (from a few minutes for **3** and **2** to over 30 min for **1** and original Rev·$0.5H_2O$) during the powder dissolution experiment (Figure S8 and Table S2, Supporting Information).

IDR is a key physicochemical parameter commonly used to assess a possible risk of the dissolution-rate controlled absorption of a new chemical entity. Owing to its kinetic nature, IDR assumes a better correlation with in vivo drug dissolution dynamics than solubility.[31] To quantitatively evaluate the impact of the solid-state modification on the dissolution behavior, in vitro dissolution studies for Rev·$0.5H_2O$ and **1**−**3** were carried out. The intrinsic dissolution


dx.doi.org/10.1021/cg500327s | *Cryst. Growth Des.* 2014, 14, 3069−3077

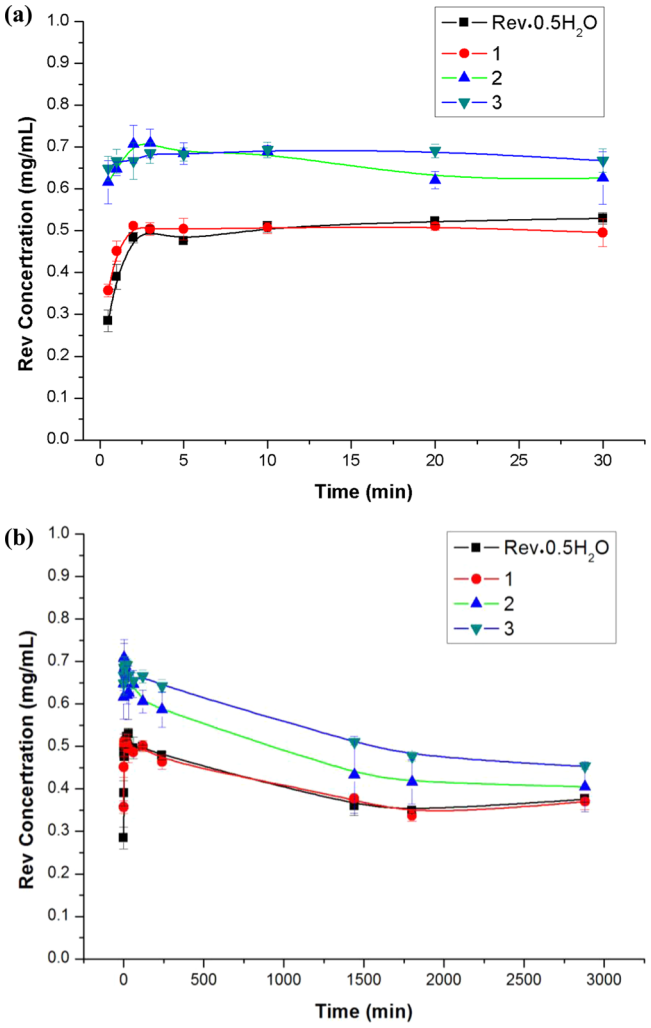


**Figure 7.** Powder dissolution profiles for Rev·0.5$H_2O$ and **1**−**3** in 0.2 M phosphate buffer of pH 6.8 at 37 °C within (a) 30 min and (b) 48 h.

profiles within the first 40 min are shown in Figure 8. It can be found that **1**−**3** show an increase in IDR as compared to original Rev·0.5$H_2O$. The IDR curve is probably a result of several processes, namely, the dissolution of the initial phase accompanied by the transition stage and followed by the slow dissolution of the newly crystallized form.[18] Such crystallinity transition behavior usually causes a nonlinearity of the IDR curve as described in details,[32] which is obviously observed for **2** and **3**. As illustrated in the powder dissolution experiment, all crystal forms would go through hemihydrate to dihydrate finally with different speeds. The undissolved solids after the IDR experiments were also analyzed by XRPD, and the results indicate that Rev·0.5$H_2O$ retained its crystal form, and **1** converts to Rev·0.5$H_2O$ while **2** and **3** transformed to Rev·2$H_2O$ (Figure S9, Supporting Information), demonstrating **2** and **3** have transformed from the initial phase to Rev·2$H_2O$ through Rev·0.5$H_2O$ intermediate within the time span for IDR (40 min), while **1** has only completed the transformation from the initial phase to hemihydrate within the same time.

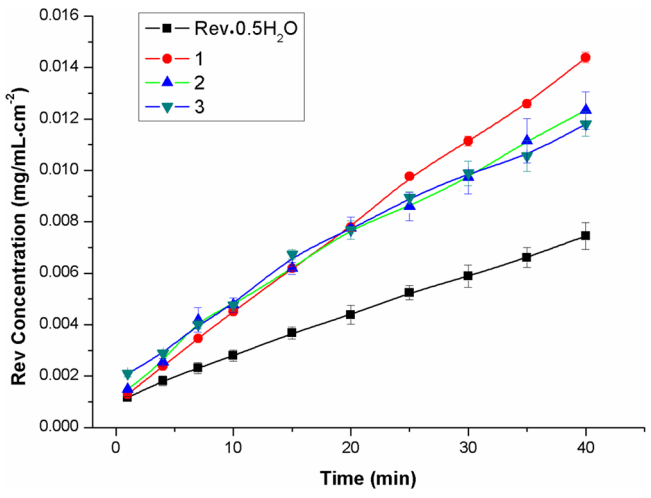


**Figure 8.** IDR profiles (first 40 min shown) for Rev·0.5$H_2O$ and **1**−**3** in 0.02 M phosphate buffer of pH 6.8 at 37 °C.

## CONCLUSIONS

Three cocrystals of **1**−**3** were synthesized, and their structures were determined. The structures of **1**−**3** are assembled via intermolecular hydrogen bonds. **2** can slowly convert to **3** in the solution containing excess of 35DHBA in the presence of water, and **3** can convert to the mixture of **2** and 35DHBA between 105 and 115 °C. The apparent solubility values and intrinsic dissolution of **2** and **3** in the phosphate buffer of pH 6.8 are larger than those of Rev·0.5$H_2O$, indicating the solubility of lenalidomide can be improved via cocrystals. As solubility and bioavailability are often related, we believe that the bioavailability of lenalidomide may also be increased after the formation of cocrystals.

## ASSOCIATED CONTENT

### Supporting Information

The coformer library used in the screening, XPRD analysis with regard to preparation, DVS, and powder and intrinsic dissolution experiments, etc. This material is available free of charge via the Internet at http://pubs.acs.org.

## AUTHOR INFORMATION

### Corresponding Authors

*(J.-M.C.) Fax: +86-20-84112921. E-mail: chenjm37@mail.sysu.edu.cn.

*(T.-B.L.) E-mail: lutongbu@mail.sysu.edu.cn.

### Notes

The authors declare no competing financial interest.

## ACKNOWLEDGMENTS

This work was financially supported by NSFC (Grant Nos. 21101173, 91127002, and 21331007), NSF of Guangdong Province (S2012030006240), and Guangzhou Pearl River New Star Fund Science and Technology Planning Project (2013J2200054).

## REFERENCES

(1) Desiraju, G. R. *Crystal Engineering. The Design of Organic Solids*; Elsevier: Amsterdam, 1989.

(2) Vangala, V. R.; Chow, P. S.; Tan, R. B. H. *Cryst. Growth Des.* **2012**, *12*, 5925−5938.

(3) Xu, L. L.; Chen, J. M.; Yan, Y.; Lu, T. B. *Cryst. Growth Des.* **2012**, *12*, 6004−6011.

(4) Valkonen, A.; Chukhlieb, M.; Moilanen, J.; Tuononen, H. M.; Rissanen, K. *Cryst. Growth Des.* **2013**, *13*, 4769−4775.

(5) Desiraju, G. R. *J. Am. Chem. Soc.* **2013**, *135*, 9952−9967.

(6) Elacqua, E.; Bučar, D.; Henry, R. F.; Zhang, G. G. Z.; MacGillivray, L. R. *Cryst. Growth Des.* **2013**, *13*, 393−403.
(7) Springuel, G.; Norberg, B.; Robeyns, K.; Wouters, J.; Leyssens, T. *Cryst. Growth Des.* **2012**, *12*, 475−484.
(8) Sanphui, P.; Goud, N. R.; Khandavilli, U. B. R.; Nangia, A. *Cryst. Growth Des.* **2011**, *11*, 4135−4145.
(9) Kola, I.; Landis, J. *Nat. Rev. Drug Discovery* **2004**, *3*, 711−715.
(10) Chen, J. M.; Wu, C. B.; Lu, T. B. *Chem. J. Chin. Univ.* **2011**, *32*, 1996−2009.
(11) Zakeri-Milani, P.; Barzegar-Jalali, M.; Azimi, M.; Valizadeh, H. *Eur. J. Pharm. Biopharm.* **2009**, *73*, 102−106.
(12) Stevens, J. S.; Byard, S. J.; Schroeder, S. L. M. *J. Pharm. Sci.* **2010**, *99*, 4453−4457.
(13) Wang, Y. C.; Feng, C. L.; Yang, S. Q.; Ji, M. *Prog. Pharm. Sci.* **2013**, *37*, 120−130.
(14) Smith, A. J.; Kavuru, P.; Wojtas, L.; Zaworotko, M. J.; Shytle, R. D. *Mol. Pharm.* **2011**, *8*, 1867−1876.
(15) Tiago, J. M.; Padrela, L.; Rodrigues, M. A.; Matos, H. A.; Almeida, A. J.; De Azevedo, E. G. *Cryst. Growth Des.* **2013**, *13*, 4940−4947.
(16) Gao, Y.; Zu, H.; Zhang, J. J. *Prog. Chem.* **2010**, *22*, 829−836.
(17) Gandhi, A.; Shi, T.; Li, M.; Jungnelius, U.; Romano, A.; Tabernero, J.; Siena, S.; Schafer, P.; Chopra, R. *PLoS One* **2013**, *8*, e80437.
(18) Yan, Y.; Chen, J. M.; Geng, N.; Lu, T. B. *Cryst. Growth Des.* **2012**, *12*, 2226−2233.
(19) Dunitz, J. D.; Gavezzotti, A. *Cryst. Growth Des.* **2012**, *12*, 5873−5877.
(20) (a) Shan, N.; Toda, F.; Jones, W. *Chem. Commun.* **2002**, 2372−2373. (b) Friscic, T.; Childs, S. L.; Rizvi, S. A. A.; Jones, W. *CrystEngComm.* **2009**, *11*, 418−426. (c) Delori, A.; Friscic, T.; Jones, W. *CrystEngComm* **2012**, *14*, 2350−2362.
(21) Sheldrick, G. M. *SHELXTL-97, Program for Crystal Structure Solution and Refinement*; University of Gottingen: Gottingen, Germany, 1997.
(22) Chen, J. M.; Wang, Z. Z.; Wu, C. B.; Li, S.; Lu, T. B. *CrystEngComm* **2012**, *14*, 6221−6229.
(23) Geng, N.; Chen, J. M.; Li, Z. J.; Lu, T. B. *Cryst. Growth Des.* **2013**, *13*, 3546−3553.
(24) Yan, Y.; Chen, J. M.; Lu, T. B. *CrystEngComm* **2013**, *15*, 6457−6460.
(25) Tao, Q.; Chen, J. M.; Lu, T. B. *CrystEngComm* **2013**, *15*, 7852−7855.
(26) Takata, N.; Takano, R.; Uekusa, H.; Hayashi, Y.; Terada, K. *Cryst. Growth Des.* **2010**, *10*, 2116−2122.
(27) Stanton, M. K.; Tufekcic, S.; Morgan, C.; Bak, A. *Cryst. Growth Des.* **2009**, *9*, 1344−1352.
(28) Takata, N.; Takano, R.; Uekusa, H.; Hayashi, Y.; Terada, K. *Cryst. Growth Des.* **2008**, *8*, 3856−3862.
(29) Cheney, M. L.; Shan, N.; Healey, E. R.; Hanna, M.; Wojtas, L.; Zaworotko, M. J.; Sava, V.; Song, S.; Sanchez-Ramos, J. R. *Cryst. Growth Des.* **2010**, *10*, 394−405.
(30) Chen, R. S.; Muller, G. W.; Jaworsky, M. S.; Saindane, M. T.; Cameron, L. M. U.S. Patent, 2005/023192, 2005.
(31) Shevchenko, A.; Bimbo, L. M.; Miroshnyk, I.; Haarala, J.; Jelínková, K. N.; Syrjänen, K.; van Veen, B.; Kiesvaara, J.; Santos, H. A.; Yliruusi, J. *Int. J. Pharm.* **2012**, *436*, 403−409.
(32) Lehto, P.; Aaltonen, J.; Tenho, M.; Rantanen, J.; Hirvonen, J.; Tanninen, V. P.; Peltonen, L. *J. Pharm. Sci.* **2009**, *98*, 985−996.